Experimental evaluation of temperature distribution of a vapor cell using a Hilbert transform procedure

He Cai, You Wang, Ming Gao, Wei Zhang, Zhigang Jiang, Juhong Han, Guofei An, Shunyan Wang, Liangping Xue, Hongyuan Wang, and Jie Zhou

Southwest Institute of Technical Physics, Chengdu, Sichuan 610041, China
(Received 9 May 2016; revised 8 August 2016; accepted 24 August 2016)

Abstract

A diode-pumped alkali vapor laser (DPAL) is one of the most promising candidates of the next-generation high-powered laser source. As the saturated number density of alkali vapor is highly dependent on the temperature inside a vapor cell, the temperature distribution in the cross-section of a cell will greatly affect the homogeneity of a laser medium and the output characteristics of a DPAL. In this paper, we developed an algorithm based on the regime concluding quasi-Hilbert transform to evaluate the phase aberration of a wavefront when the probe beam passes through the vapor cell placed in one arm of a Mach–Zehnder interference setup. According to the theoretical algorithm, we deduced the temperature distribution of a cesium vapor cell for different heating conditions. The study is thought to be useful for development of a high-powered laser.

Keywords: DPAL; Hilbert transform; temperature distribution; vapor cell

1. Introduction

The concept of a diode-pumped alkali vapor laser (DPAL) was first proposed by Krupke in Lawrence Livermore National Laboratory (LLNL) at the beginning of the twenty-first century[1]. In the past decade, DPALs have been paid a lot of attention because of their advantages of high Stokes efficiency, good beam quality, compact size and near-infrared emission wavelengths[2–4]. However, the temperature inside the vapor cell in a DPAL system usually exhibits an inhomogeneous distribution due to the poor thermal conductivity of a gas-state medium. Such a phenomenon would influence the conversion efficiency as the number intensity of the gain medium is only determined by the cell temperature[5, 6]. Therefore, it is essential to investigate the temperature distribution inside a vapor cell, especially for construction of a high-powered DPAL system with good beam quality.

Till now, some theoretical analyses have been carried out to evaluate the temperature distribution of an alkali vapor cell. Pan *et al.* have established a physical model based on the theory of heat transfer to calculate the temperature distribution at different pump powers[7]. Based on the kinetic evaluation, Barmashenko *et al.* have calculated the temperature distribution by assuming the temperature is a constant inside the lasing region[8]. Han *et al.* have created an analytic system by considering both laser kinetics and heat transfer[9–11]. Shaffer has presented a new method to measure the temperature in a Cs cell, in which the simulation process is greatly dependent on a software called as QuickFringe[12]. The experimental results of the temperature distribution at the cross-section of a sealed cell containing the alkali vapor medium have been rare so far. In this study, we introduce an algorithm to evaluate the temperature distribution in the cross-section of a heated vapor cell with help of a procedure containing quasi-Hilbert transform, which has been commonly used to retrieve the wavefront aberration from interferograms with desired measurement precision[13–16]. Based on the theoretical analyses, we deduced the temperature distribution inside a vapor cell which had been positioned beforehand in one arm of a Mach–Zehnder interferometer. The study provides a feasible way to investigate the temperature features of a laser medium.

2. Methodological description

In this section, we mainly introduce a theoretical algorithm to calculate the temperature distribution of a vapor cell from the interferometric phase images. The analysis processes, which are divided into two steps, are respectively presented in Sections 2.1 and 2.2.

Correspondence to: Y. Wang, Southwest Institute of Technical Physics, Renmin South Road 4-7, Chengdu, Sichuan 610041, China. Email: youwang_2007@aliyun.com
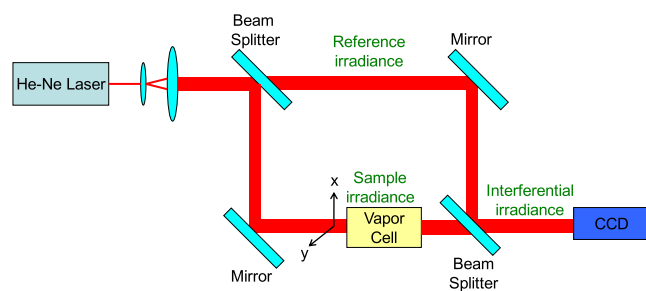
Figure 1. Schematic diagram of the experimental setup.

Figure 2. Wavefront distribution caused by manufacture defects of two cell side windows.

2.1. Simulation of the phase aberration using a quasi-Hilbert transform

Figure 1 shows the schematic diagram of a Mach–Zehnder interferometer setup in the experiment. A He–Ne laser is employed as the probe laser whose beam size is enlarged by an inversed telescopic system. The vapor cell (4 cm length, 1.5 cm diameter), in which 500 Torr methane was beforehand filled at the room temperature, is placed in one arm of the Mach–Zehnder interferometer. During the experiment, a heater was used to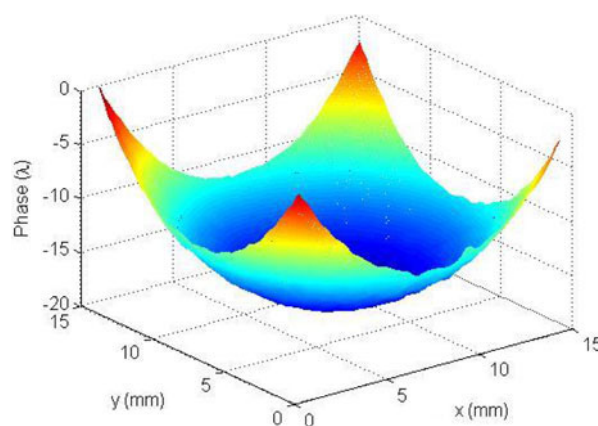 warm the cell and a thermocouple was employed to detect the temperature on the outside surface of a cell. Employing a CMOS camera with a 4f-optical imaging system, we record intensity distributions of the sample beam, reference beam, and interferential pattern at different heating conditions. Thus, the interferential irradiance intensity at the camera can be written as[16]
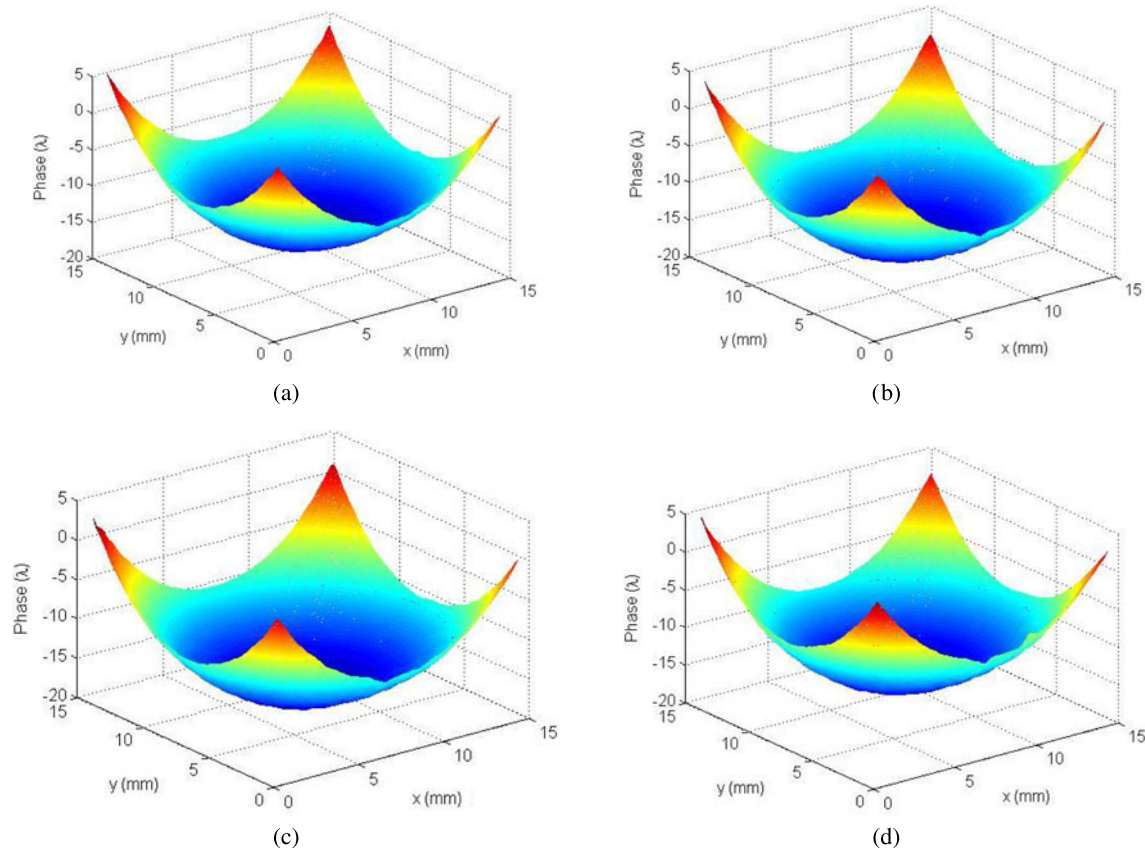

(a)

(b)

(c)

(d)

Figure 3. Wavefront distributions associated with the vapor cell when the temperatures of the heater are (a) 60 °C, (b) 80 °C, (c) 100 °C and (d) 120 °C, respectively.
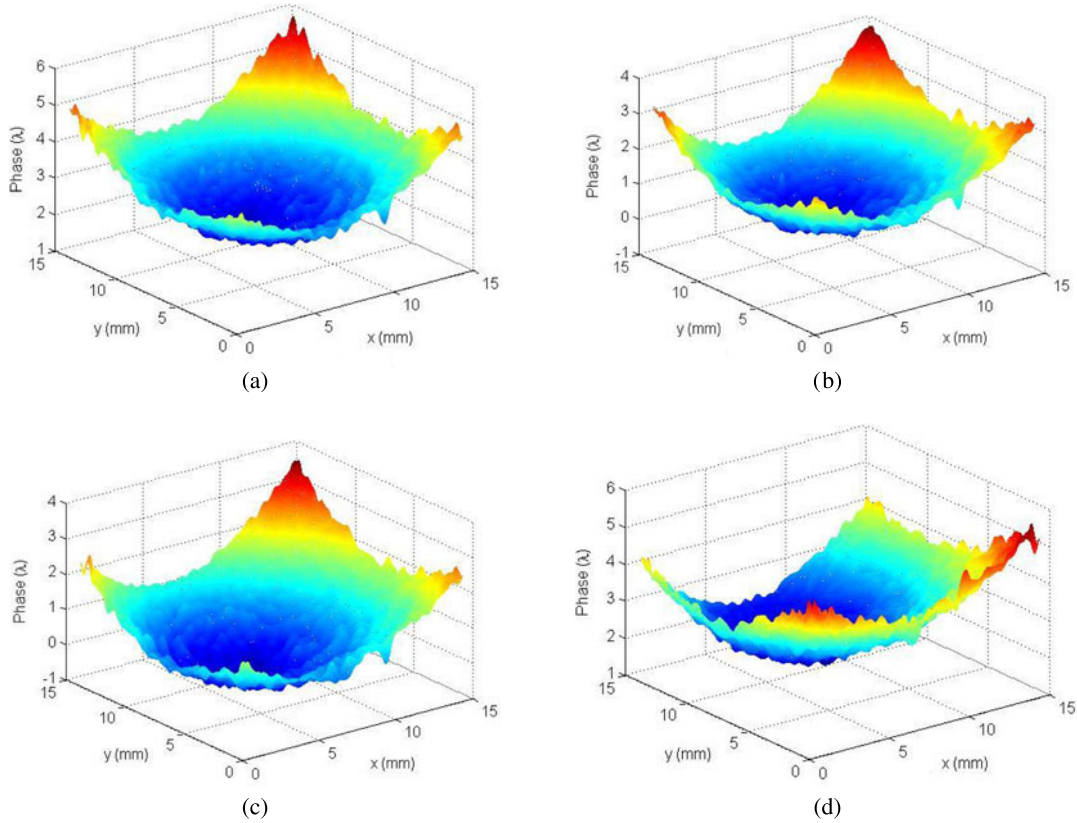
Figure 4. Wavefront distributions induced by the gas medium when the heater temperatures are (a) 60 °C, (b) 80 °C, (c) 100 °C and (d) 120 °C, respectively.

$$I_{CCD}(x, y) = I_S(x, y) + I_R(x, y)$$
$$+ 2\sqrt{I_S(x, y) \cdot I_R(x, y)}$$
$$\cdot \cos[\phi(x, y) + (q_x x + q_y y)], \quad (1)$$

where $I_S(x, y)$ and $I_R(x, y)$ are the sample and reference beam intensities, $\phi(x, y)$ is the spatial phase associated with the cell, q_x and q_y are the spatial frequencies of the interference fringes, respectively. Note that $\phi(x, y)$ is a parameter that we most concern about in this subsection.

Solving Equation (1), we can get a cosine term as expressed by

$$\cos[\phi(x, y) + (q_x x + q_y y)]$$
$$= \frac{I_{CCD}(x, y) - [I_S(x, y) + I_R(x, y)]}{2\sqrt{I_S(x, y) \cdot I_R(x, y)}}. \quad (2)$$

Next, the cosine term is changed to frequency domain by means of a procedure of fast Fourier transform (FFT):

$$F(u, v) = \text{FFT}(\cos[\phi(x, y) + (q_x x + q_y y)]). \quad (3)$$

Then, the low frequency background noise and one of the conjugate patterns in $F(u, v)$ are removed by use of a bandpass filter. After that, we can have a new function

through an inverse fast Fourier transform (IFFT)[13]:

$$z(x, y) = \tfrac{1}{2} \cos[(q_x x + q_y y) + \phi(x, y)]$$
$$+ i \cdot HT \left\{ \tfrac{1}{2} \cos[(q_x x + q_y y) + \phi(x, y)] \right\}, \quad (4)$$

where the imaginary part of the right side of the above equation stands for the Hilbert transform of the real part, which is presented by

$$HT \left\{ \tfrac{1}{2} \cos[(q_x x + q_y y) + \phi(x, y)] \right\}$$
$$= \tfrac{1}{2} \sin[(q_x x + q_y y) + \phi(x, y)]. \quad (5)$$

By combining Equations (4) and (5), we can calculate the value of a wrapped phase in the range of $-\pi$ and π as expressed by

$$\Phi(x, y) = \arctan\left(\frac{\text{Im}[z(x, y)]}{\text{Re}[z(x, y)]} \right). \quad (6)$$

Finally, the phase distortion associated with the vapor cell can be retrieved by an unwrapping theme and an incline correction procedure by using the calculation as follows:

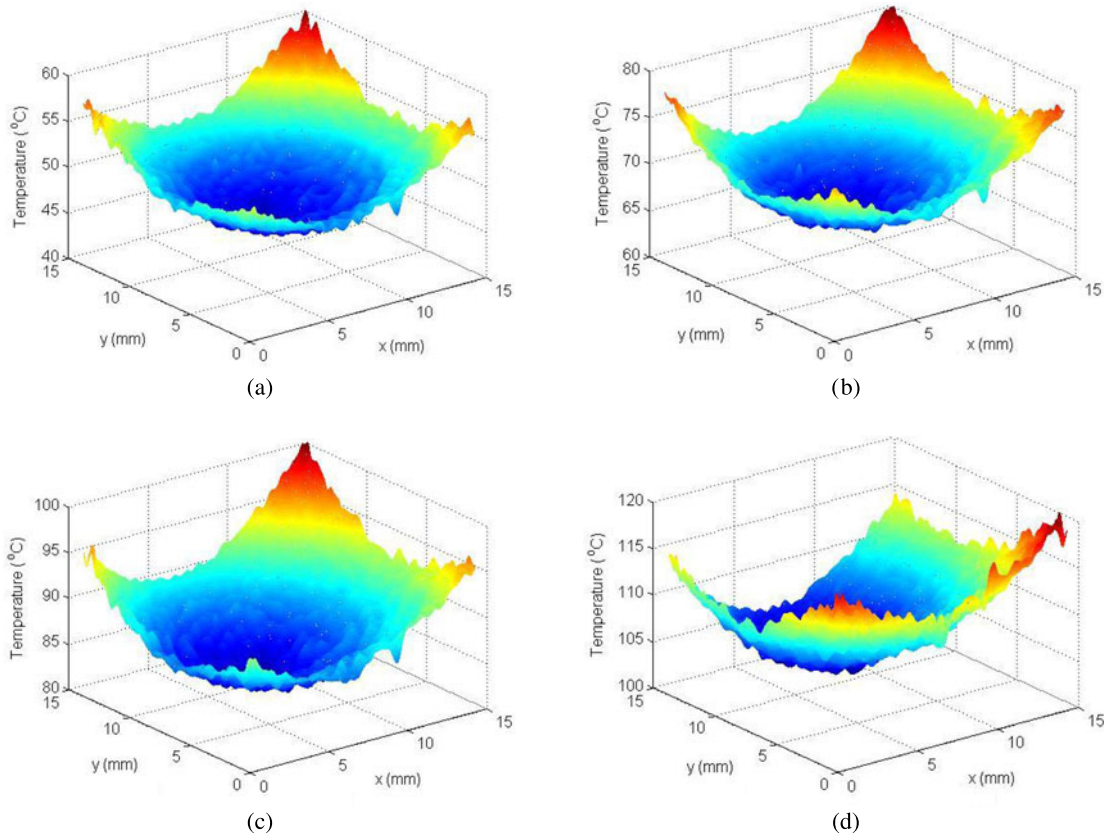$$\phi(x, y) = \Phi(x, y) - (q_x x + q_y y). \quad (7)$$

Figure 5. Temperature distributions at the cross-section of a vapor cell when the heater temperatures are (a) 60 °C, (b) 80 °C, (c) 100 °C and (d) 120 °C, respectively.

2.2. Evaluation of the temperature distribution inside a vapor cell

Next, we focus on evaluating the temperature distribution in the cross-section of a cell while the temperature distribution is assumed to be uniform along the longitudinal axis. Thus, the optical path length $L(x, y)$ in waves for the probe laser can be expressed by

$$L(x, y) = L_{\text{cell}} k n(x, y), \qquad (8)$$

where L_{cell} is the length of a vapor cell, k stands for the wavenumber of the probe laser, and $n(x, y)$ is the refractive index distribution inside a cell, respectively.

Generally, the temperature distribution will become nonuniform when the cell is heated. Nevertheless, the temperature at the cell edge can be directly measured through a commercial thermocouple. Thus, when a probe laser passes through the vapor cell, the phase difference of a wavefront is expressed by

$$\Delta N(x, y) = L(x, y) - L_{\text{edge}} = L_{\text{cell}} k n(x, y) - L_{\text{cell}} k n_{\text{edge}}, \qquad (9)$$

where L_{edge} and n_{edge} are the length in waves and the refractive index at the edge of a vapor cell. $\Delta N(x, y)$ can be

calculated by the theory introduced in last subsection with the following formula:

$$\Delta N(x, y) = \phi(x, y) - \phi_{\text{edge}}, \qquad (10)$$

where ϕ_{edge} is the spatial phase at the edge of a vapor cell. According to the ideal gas law and the Gladstone–Dale relation, the relationship between the temperature of the arbitrary point at the cross-section and that at the cell edge yields[12]

$$T(x, y) = T_{\text{edge}} \frac{n_{\text{edge}} - 1}{n(x, y) - 1}. \qquad (11)$$

Uniting Equations (9) and (11), we can obtain the temperature distribution of a heated cell expressed by

$$T(x, y) = T_{\text{edge}} \frac{n_{\text{edge}} - 1}{n_{\text{edge}} - 1 + \frac{\Delta N(x, y)}{L_{\text{cell}} k}}. \qquad (12)$$

3. Results and discussions

Using the principle of theoretical analyses, we can deduce the temperature distribution of a cesium vapor cell at dif-

ferent heating conditions. We first evaluate the wavefront aberration caused by manufacture deviations of both side windows of the cell. The result is represented in Figure 2. We can see that the wavefront exhibits a curved surface rather than a flat plane after the probe laser beam passes through a vapor cell. Actually, both cell windows present features like two concave lenses, which is caused by the fusing process during the cell fabrication. Here, it is extremely necessary to compute the wavefront aberration arising from the side windows because such a term will bring about a non-negligible error for evaluation of the temperature simulation.

Figure 3(a)–(d) show the calculated wavefront distributions from Equation (7) when the temperatures of the heater were raised to 60 °C, 80 °C, 100 °C and 120 °C, respectively. Note that Figure 3(a)–(d) are obtained by using the data just at the time when the temperature at the cell edge reaches the setting value. Removing the influence of both side windows as shown in Figure 2, only the wavefront aberrations induced by the heated gas medium can be obtained as shown in Figure 4(a)–(d). Then, we evaluated the temperature distributions referring to Figure 5(a)–(d) by use of Equation (12). We can see that the temperature in the center area is always lower than that at the cell edge. The maximum temperature difference at the cross-section of the cell ranges from 15 °C to 18 °C. The large temperature gradient also verifies that the thermal conductivity of the gas medium inside the cell is relatively low. The study offers a useful means to compensate the wavefront aberration of a high-powered DPAL system by monitoring the real-time thermal feature inside a vapor cell.

4. Summary

In this study, we introduce a new algorithm to deduce the temperature distribution of an alkali vapor cell using a procedure containing quasi-Hilbert transform. Besides development of the theoretical regime, we also construct a Mach–Zehnder interferometer to experimentally deduce the temperature distribution of a cesium vapor cell at different heating conditions. The results reveal that the temperature distribution is inhomogeneous at the cross-section of an annealed alkali vapor cell. Next, we will apply this technique to analyze the thermal gradients of an alkali vapor cell pumped by laser diodes. We also believe the algorithm should be helpful to investigate the thermal effects of a high-powered laser system especially when pump beams have been turned on and the system is lasing in the future.

References

1. W. F. Krupke, US Patent Application, 0099272 Al (2003).
2. R. J. Beach, W. F. Krupke, V. K. Kanz, and S. A. Payne, J. Opt. Soc. Am. B **21**, 2151 (2004).
3. Y. Wang, T. Kasamatsu, Y. Zheng, H. Miyajima, H. Fukuoka, S. Matsuoka, M. Niigaki, H. Kubomura, T. Hiruma, and H. Kan, Appl. Phys. Lett. **88**, 141112 (2006).
4. W. Zhang, Y. Wang, H. Cai, L. P. Xue, J. H. Han, H. Y. Wang, and Z. Y. Liao, App. Opt. **53**, 4180 (2014).
5. Z. N. Yang, H. Y. Wang, Q. S. Lu, W. H. Hua, and X. J. Xu, Opt. Lett. **19**, 23118 (2011).
6. D. A. Steck, Rubidium 85 D Line Data. Available online at http://steck.us/alkalidata.
7. Q. Zhu, B. L. Pan, L. Chen, Y. J. Wang, and X. Y. Zhang, Opt. Commun. **283**, 2406 (2010).
8. B. D. Barmashenko and S. Rosenwaks, Opt. Lett. **37**, 3615 (2012).
9. J. H. Han, Y. Wang, H. Cai, W. Zhang, L. P. Xue, and H. Y. Wang, Opt. Express **22**, 13988 (2014).
10. J. H. Han, Y. Wang, H. Cai, G. F. An, W. Zhang, L. P. Xue, H. Y. Wang, J. Zhou, Z. G. Jiang, and M. Gao, Opt. Express **23**, 9508 (2015).
11. W. Zhang, Y. Wang, H. Cai, L. P. Xue, J. H. Han, H. Y. Wang, and Z. Y. Liao, Appl. Opt. **53**, 4180 (2014).
12. M. K. Shaffer, T. C. Lilly, B. V. Zhdanov, and R. J. Knize, Opt. Lett. **40**, 119 (2015).
13. T. Ikeda, G. Popescu, R. R. Dasari, and M. S. Feld, Opt. Lett. **30**, 1165 (2005).
14. R. J. Green, J. G. Walker, and D. Robinson, Opt. Laser Eng. **8**, 29 (1988).
15. C. Quan, H. M. Shang, and P. J. Bryanston-Cross, Opt. Laser Technol. **28**, 7 (1996).
16. W. O. Wong and T. T. Chan, Opt. Laser Technol. **30**, 317 (1998).